Metastability of Microtubules Induced by Competing Internal Forces

Viktória Hunyadi and Imre M. Jánosi
Department of Physics of Complex Systems, Eötvös University, Pázmány Péter s. 1/A, H-1117 Budapest, Hungary

ABSTRACT Recent modeling efforts to estimate energies of tubulin-tubulin bonds shed light on a delicate balance between competing mechanical forces maintaining microtubule walls. Here we formulate two important refinements to the explanation of bond energetics. First, energy surface calculations in the elastic filament approximation reveal a finite stabilizing barrier assumed a simple Lennard-Jones-like potential for protein bonds. The presence of a guanosine triphosphate (GTP) cap represented by straight segments is necessary, as it is predicted for a long time. In the lack of such a cap, the protofilaments are either in an absolutely stable or absolutely unstable state. Second, our calculations show that this barrier appears only if the mechanical energy associated with the conformational change after GTP hydrolysis (curling energy) is larger than the strength of lateral bonds. The overall energy balance we propose supports continuous assembly of GTP dimers, a metastable state in the presence of a finite GTP cap and energetically driven disassembly of guanosine diphosphate protofilaments.

INTRODUCTION

Tubulin α-β dimers in a microtubule (MT) are most frequently arranged in 13 protofilaments aligned parallel to the central axis (1). When MTs depolymerize, these protofilaments curve outward as a consequence of a conformational change, which is triggered by the hydrolysis of guanosine triphosphate (GTP) bound to β-tubulin. Direct evidence of this long assumed conformational change has been recently presented by Wang and Nogales (2). They found that in guanosine diphosphate (GDP)-bound dimers, the contacts between the α- and β-tubulins within and between dimers are both affected, resulting in a curved protofilament that cannot form lateral contacts.

According to the ''traditional'' thermodynamic-kinetic view, GTP-bound tubulin subunits have a high affinity for MT ends, promoting persistent MT growth, whereas GDP-bound tubulin dimers have a low affinity and dissociate quickly. A kinetic lag between polymerization and hydrolysis could generate a ''GTP cap'' formed by almost straight GTP dimers, which is presumed to stabilize growing ends (3).

A crucial question in understanding dynamic instability (the random switch between continuous growth and rapid shortening) is how the chemical energy from GTP hydrolysis is exploited to power both growth and shrinkage of MTs. Recent modeling studies, especially by VanBuren et al. (4,5) and Molodtsov et al. (6,7), seem to reach a conclusion on quantitative aspects of bond energetics of the MT wall.

The stability of an MT is determined by the bonds between tubulin subunits forming the wall lattice. It is plausible to characterize the strength of bonds by energy parameters associated with the depth of (not precisely known) potentials of protein-protein interaction. For a particular subunit, the energetic balance (total energy), E_{tot}, contains at least three terms: net longitudinal bond energy, E_{long}; effective lateral bond energy, E_{lat}; and curling energy, E_{c}. (Note that any effect of possible external deformations is omitted in the following considerations.)

The individual terms in the energy balance for tubulin subunits have been estimated by various methods. First of all, stochastic modeling of the chemical kinetics (4) yields an estimate of $E_{\mathrm{tot}}^{\mathrm{GTP}} \approx -12.5\ k_{\mathrm{B}}T$ per dimer for the net standard free-energy promoting spontaneous assembly of GTP tubulin (k_{B} is the Boltzmann constant, and T is the absolute temperature in the physiological range). This estimate is further supported by a different study on energetically unfavorable MT configurations, concluding that the stabilizing free-energy is around $E_{\mathrm{tot}} \approx -10.5\ k_{\mathrm{B}}T$ per dimer for 13 protofilament GDP MTs (8). Note that the difference between $E_{\mathrm{tot}}^{\mathrm{GTP}}$ and E_{tot} can be attributed to the contribution of internal curling triggered by the hydrolysis step (see below).

Second, depending on the assembly rate constant, longitudinal and lateral bond energies are estimated by the stochastic assembly model in VanBuren et al. (4) (Table 1). The free-energy shift associated with the conformational change after GTP hydrolysis is estimated at 2.1–2.5 $k_{\mathrm{B}}T$/dimer by pure kinetic modeling (4) and 3.7–4.2 $k_{\mathrm{B}}T$/dimer by considering flexural rigidity and measured shortening velocities (5). Similar energy values are difficult to extract from the molecular-mechanical model of Molodtsov et al. (6) and Molodtsov et al. (7) because the parameterization of interactions has no direct link to measured absolute values (e.g., longitudinal bonds are not represented by any potential; they are not extensible and do not break).

All these models agree in the crucial point that the existence of a stabilizing GTP cap of reduced internal curvature is necessary to prevent MTs from disassembly (4–7). Such a GTP cap is thought to determine MT stability for a long time (9–12).

The helical dimer arrangement in the lateral direction (1) has a negligible effect on the overall MT stability and mechanical properties, as demonstrated in Molodtsov et al. (6).

Submitted June 20, 2006, and accepted for publication January 4, 2007.

Address reprint requests to Imre M. Jánosi, E-mail: janosi@lecso.elte.hu.

0006-3495/07/05/3092/06 $2.00

doi: 10.1529/biophysj.106.091793

TABLE 1 Estimated bond energies for different rates of tubulin dimer association ($k_{(+)}$)

	$k_{(+)}$ [$\mu M^{-1}s^{-1}$]	E_{lat} [k_BT/dimer]	E_{long} [k_BT/dimer]	E_c [k_BT/dimer]	Reference
(i)	2	−3.2	−9.4	2.1	(4)
(ii)	4	−5.7	−6.8	2.5	(4)
(iii)	2	−3.2	−9.4	3.7	(4,5)
(iv)	4	−5.7	−6.8	4.2	(4,5)

The curling energy (E_c) is assessed by a stochastic kinetic model in VanBuren et al. (4) and by matching measured flexural rigidity and disassembly rates in VanBuren et al. (5).

We will exploit this result in our calculations by considering a single protofilament in a laterally symmetric effective environment.

In this work we refine this picture by two main points. First, we explicitly show that a finite energy barrier can naturally arise from the superposition of a simple quadratic bending- and a Lennard-Jones-like bonding potential. A single GTP tubulin ring at the growing end is necessary and sufficient to maintain a metastable equilibrium, in agreement with many earlier predictions. Second, we illustrate that the driving force of rapid disassembly is easily available when the conformational change destabilizes the lattice, i.e., intrinsic bending forces can break lateral bonds.

Energy contour calculations

We performed computations by means of the elastic filament approximation described in Jánosi et al. (13). In this model, a protofilament is considered as a discretized one-dimensional string bound laterally to neighboring filaments. The tubular symmetry allows a simplified description of lateral bonds by an effective radial potential. Such a filament obeys also a longitudinal bending constraint represented by a nonzero intrinsic curvature for GDP segments and a quadratic potential associated with it. Longitudinal and lateral bonds can be characterized by Lennard-Jones potentials (Fig. 1):

$$V_{LJ}(r) = V_0\left[\left(\frac{r_0}{r}\right)^{12} - 2\left(\frac{r_0}{r}\right)^{6}\right], \quad (1)$$

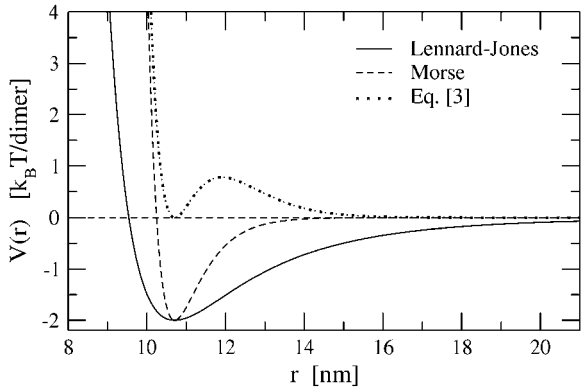

FIGURE 1 Potential functions implemented in the energy map calculations; see Eqs. 1–3. Parameters are given in Figs. 2–4.

where V_0 is the depth of the potential valley located at r_0. We also tested the Morse potential, which has a shape very similar to V_{LJ} with an adjustable width parameter δ (see Fig. 1):

$$V_M(r) = V_0[e^{-2\delta(r-r_0)} - 2e^{-\delta(r-r_0)}]. \quad (2)$$

Here r_0 and V_0 are identical to those in Eq. 1, $\delta \approx 5/r_0$ reproduces more or less the corresponding Lennard-Jones shape, and larger values result in much narrower potential valleys. These forms are to be compared with the potential function implemented for lateral bonds by Molodtsov et al. (6,7):

$$V(r) = A(r - r_0)^2 e^{-\lambda(r-r_0)}, \quad (3)$$

where r_0 defines the location of potential energy minimum again, and λ is a parameter characterizing the distance and relative height of the built-in energy barrier (see Fig. 1). Such potential entails an ''automatic'' bond breaking for large enough $(r - r_0)$ spatial separations. Note that an additional term to Eq. 3 easily produces a negative minimum together with an asymptotic zero value (for details, see Molodtsov et al. (6,7)); however this gives only an additive shift in the final energy balance (6). The principal difference between Eq. 3 and the Lennard-Jones-like potentials in Eqs. 1 and 2 is that the former has a long-range repulsive regime, which is not really supported by computed (14–17) or measured (18) results.

We note that VanBuren et al. implemented simple quadratic potentials for each bonds in their mechanochemical model (5); bond breaking was realized ''by hand'' when external mechanical forces exceeded critical values.

We have computed energy contour maps for elastic filaments represented by a longitudinally joined sequence of straight rods with one clamped and one free terminal. For the sake of simplicity, only radial deflections were considered, as they manifest the lowest energy deformation modes. Longitudinal and lateral bonds were characterized by Lennard-Jones or Morse potentials, and bending constraints were implemented by a prescribed equilibrium angle between segments (22°) and a quadratic potential. The very end of the free terminal was forced to have a fixed spatial position, and then the filament was allowed to be relaxed by global conjugate gradient minimization (see, e.g., Jánosi et al. (19)). The resulting minimum energy was utilized to construct contour maps reflecting energetic stability (Figs. 2

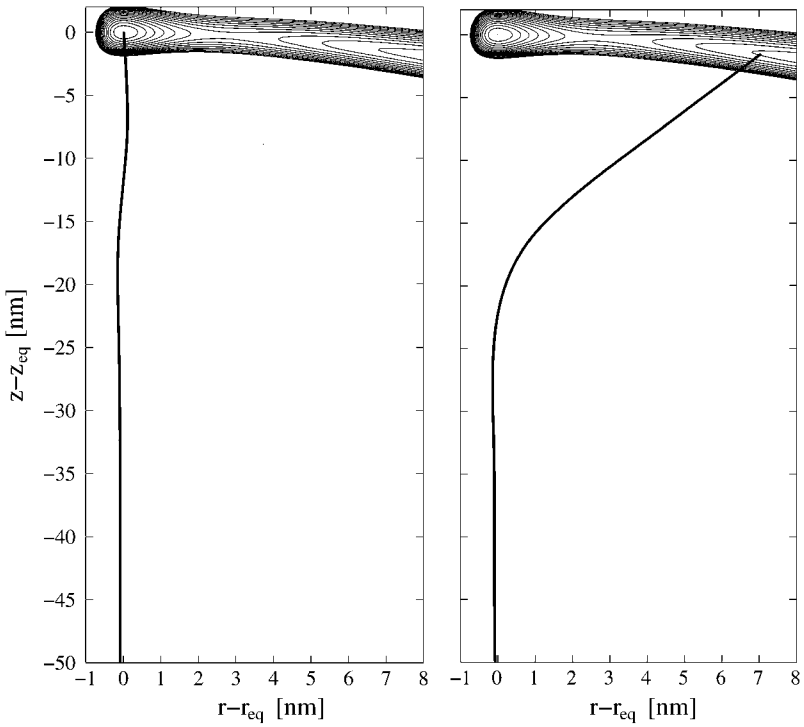

FIGURE 2 Illustration of the energy contour map calculation. (*Left*) Relaxed filament configuration with a unit cap defines the equilibrium position of the free terminal. (*Right*) The very end is forced to a given position, and the filament is allowed to relax into a minimal energy configuration. The final energy is used to draw contour lines. (The horizontal axes are lengthened; units are in nm.) Parameters: Morse potential, $E_{tot} = -10.5\ k_BT$/dimer, $E_c = +3.0\ k_BT$/dimer, $E_{lat} = -2.0\ k_BT$/dimer, $\delta = 1.12\ nm^{-1}$.

and 3). Note that this energy is not normalized by the number of segments; it measures the difference between the relaxed global minimum value and the energy of a given forced configuration for a filament of arbitrary length.

The parameters of the potentials were tuned to have a minimum at the effective tube radius $r_0 = 10.72$ nm and at the equilibrium dimer length of 8.08 nm (see, e.g., Chrétien and Fuller (1)). The numerical value for total energy, $E_{tot} = -10.5\ k_BT$, per segment was set for a GDP unit buried deep in the MT wall, following VanBuren et al. (4) and Hunyadi et al. (8).

The effects of a GTP cap were modeled by setting the equilibrium angle to 0° (perfectly straight limit) or 5° (see Wang and Nogales (2)) with the same bond energy parameters for a few top segments of a filament. Note that such a finite cap does not necessarily adopt a straight equilibrium configuration (see Fig. 2 *a*) because some curling deformation propagates upward from the GDP parts below (6,13).

RESULTS AND DISCUSSION

Representative energy maps are shown in Fig. 3. We have scanned Lennard-Jones and Morse potentials with various (E_{long}, E_{lat}, and E_c) combinations by keeping the value of E_{tot} fixed and with straight cap segments of 0–4 units. The spatial resolution of the mapping was $\Delta r = \Delta z = 0.1$ nm in both directions. The curling energy, E_c, and the lateral bond strength, E_{lat}, were changed in the range 1–10 k_BT/dimer (E_{long} automatically arises from the balance). Combinations giving finite, positive resulting energy barriers are listed in Table 2 for Lennard-Jones potentials with unit and two-unit caps.

The main results can be summarized as follows:

1) In the case of pure GDP filaments, the necessary condition for a stable tube configuration is $|E_{lat}| > E_c$. This plausible requirement was also demonstrated in Molodtsov et al. (6). We found that such energy balance always yields to an absolutely stable equilibrium with Lennard-Jones or Morse potentials, as shown in Fig. 3, top. When the relationship is reversed, $|E_{lat}| < E_c$, the filament is absolutely unstable: it always curls up spontaneously.
2) Our calculations explicitly show that a metastable equilibrium is possible with $|E_{lat}| < E_c$ in the presence of a GTP cap (at least one straight segment). In this case, an energy barrier appears as shown in Fig. 3, middle and bottom. The height and location of the barrier depends on the type and parameters of the potentials and the length of the cap segment (see Table 2 and Figs. 3 and 4). Largest barriers arise with long caps or narrow potential valleys at small differences between curling and lateral bond energies.
3) Metastability breaks down when the curling energy, E_c, overly exceeds $|E_{lat}|$. This limit is indicated by a steeply decreasing barrier height (illustrated in Fig. 5). The calculated critical lines are depicted in Fig. 6 both for Lennard-Jones and Morse potentials with various cap sizes.

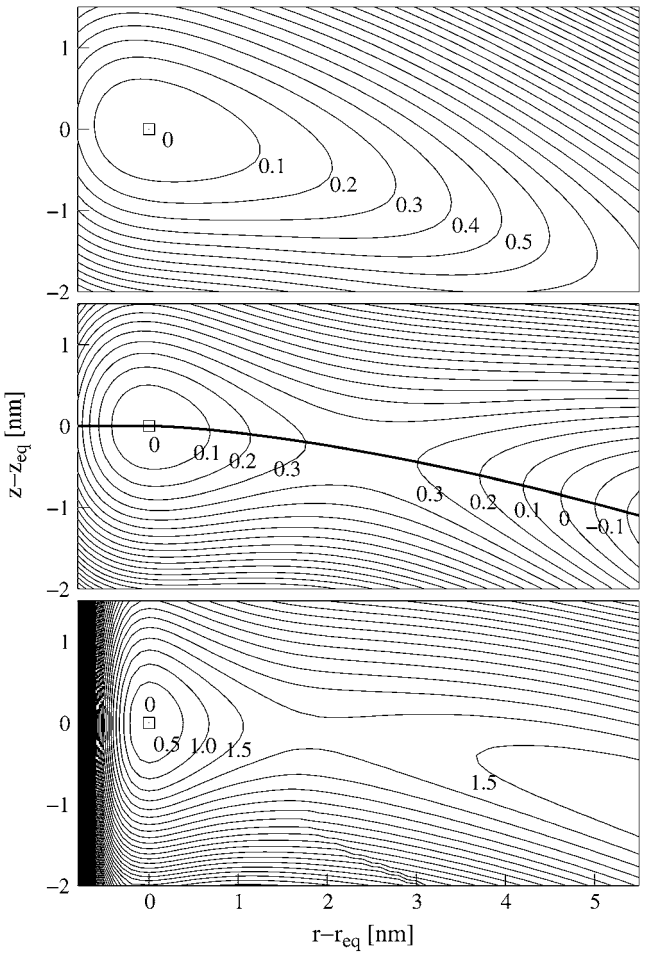

FIGURE 3 Energy contours (in units of k_BT) for a filament of 40 units as a function of the spatial separation from the spontaneous equilibrium terminal position (r_{eq}, z_{eq}) denoted by a heavy dot. (*Top*) Lennard-Jones bond potentials (1), with parameters from VanBuren et al. (4,5): $E_{long} = -9.4\ k_BT$/dimer, $E_{lat} = -3.2\ k_BT$/dimer, and $E_c = +2.1\ k_BT$/dimer, without GTP cap. (*Middle*) Lennard-Jones bond potentials, $E_{long} = -11.5\ k_BT$/dimer, $E_{lat} = -2.0\ k_BT$/dimer, and $E_c = +3.0\ k_BT$/dimer, with one unit of GTP cap. (The *heavy line* indicates the ridge where the resulting potential is reconstructed in Fig. 4.) (*Bottom*) Morse potentials, the same bond parameters as in the middle, $\delta = 1.85\ nm^{-1}$, with one unit of GTP cap.

TABLE 2 The height E_b and location (Δr,Δz) of the energy barrier for a filament with unit and two-unit GTP caps (under the line)

E_c	E_{lat}	E_{long}	E_b [k_BT]	Δr [nm]	Δz [nm]
3.0	−2.0	−11.5	0.23	3.1	−0.4
4.0	−3.0	−11.5	0.66	4.1	−0.7
5.0	−3.0	−12.5	0.12	2.0	−0.3
5.0	−4.0	−11.5	1.14	4.9	−0.9
6.0	−4.0	−12.5	0.46	2.9	−0.4
6.0	−5.0	−11.5	1.65	5.5	−1.1
7.0	−4.0	−13.5	0.06	1.4	−0.2
7.0	−5.0	−12.5	0.87	3.6	−0.6
7.0	−6.0	−11.5	2.17	6.0	−1.2
8.0	−5.0	−13.5	0.33	2.3	−0.3
8.0	−6.0	−12.5	1.32	4.1	−0.7
8.0	−7.0	−11.5	2.69	6.5	−1.4
9.0	−5.0	−14.5	0.02	1.0	−0.1
9.0	−6.0	−13.5	0.69	3.0	−0.4
9.0	−7.0	−12.5	1.79	4.5	−0.8
9.0	−8.0	−11.5	3.23	7.0	−1.6
10.0	−6.0	−14.5	0.24	1.9	−0.3
10.0	−7.0	−13.5	1.09	3.4	−0.5
10.0	−8.0	−12.5	2.28	4.9	−0.9
10.0	−9.0	−11.5	3.78	7.5	−1.8
2.0	−1.0	−11.5	0.62	5.2	−0.6
3.0	−1.0	−12.5	0.15	2.6	−0.2
3.0	−2.0	−11.5	1.98	7.6	−1.2
4.0	−2.0	−12.5	1.24	5.2	−0.6
4.0	−3.0	−11.5	3.43	9.0	−1.6
5.0	−2.0	−13.5	0.70	3.7	−0.3
5.0	−3.0	−12.5	2.56	6.6	−0.9
5.0	−4.0	−11.5	4.92	10.1	−2.0
6.0	−2.0	−14.5	0.31	2.6	−0.2
6.0	−3.0	−13.5	1.86	5.2	−0.6
6.0	−4.0	−12.5	3.95	7.6	−1.2
7.0	−2.0	−15.5	0.05	1.4	−0.1
7.0	−3.0	−14.5	1.29	4.2	−0.4
7.0	−4.0	−13.5	3.15	6.2	−0.8
7.0	−5.0	−12.5	5.38	8.3	−1.4
8.0	−3.0	−15.5	0.83	3.3	−0.3
8.0	−4.0	−14.5	2.48	5.2	−0.6
8.0	−5.0	−13.5	4.52	6.9	−1.0
8.0	−6.0	−12.5	6.85	9.1	−1.7

Lennard-Jones potential, $E_{tot} = -10.5\ k_BT$/dimer. Results for the unit cap cases are plotted in Fig. 5.

Since the particular functional form and the parameters of the effective tubulin bond potentials are not known, we do not formulate quantitative predictions. The simple filament model certainly gives unrealistic values for the location of barrier maxima, especially with Lennard-Jones potentials. Nevertheless we think that our results are essential from a conceptual point of view.

An energy barrier implicitly arises with ''realistic'' bond potentials (without built-in or ''handmade'' bond breaking) in the presence of a single straight or moderately curved segment. The parameter sets we found support both continuous MT growth with a GTP cap ($E_{tot} < 0$) and energetically driven spontaneous disassembly of GDP protofilaments. The essential point is the possibility of $|E_{lat}| < E_c$ in this case bending forces alone can break lateral bonds in the GDP state. Such bond breaking is possible only at the tube terminals; GDP units deeply inside the wall are fixed by longitudinal bonds (kinetic barrier). This picture suggests that catastrophes can occur also in the case of strong enough thermal fluctuations; the complete loss of the GTP cap is not a precondition.

We emphasize that the values of prescribed equilibrium angles are not important for the existence of metastable equilibrium, whenever their difference is large enough. When the GTP segments are assumed to not be perfectly straight, e.g., the intrinsic angle is 5° (2), the domain of metastability shrinks by ~10% in the maps shown in Fig. 6.

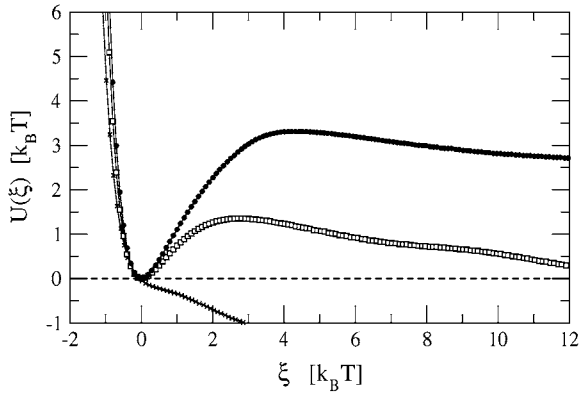

FIGURE 4 Reconstruction of the energy barrier (along similar ridges indicated in Fig. 3 *middle* by a *heavy line*) for Morse potential maps with $E_{long} = -11.5\ k_BT$/dimer, $E_{lat} = -2.0\ k_BT$/dimer, and $E_c = +3.0\ k_BT$/dimer, $\delta = 1.12\ nm^{-1}$. Changing parameter is the cap size: no cap (*crosses*), unit cap (*open squares*), two-unit cap (*solid circles*).

Similarly, the parameter values for longitudinal bonds do not affect the general behavior. This is because the model here intends to capture the initial phase of disassembly characterized by the famous ''ram's horn'' configuration: protofilaments are curling off, but longitudinal bonds are not broken yet. The parameter values $E_{long} < 0$ do not permit fast disassembly of single protofilaments. Such delay between the lateral and longitudinal bond-breaking events is supported by the observation of many curled short GDP tubulin segments in a solution after MT catastrophes (21).

Our results are not in full agreement with some conclusions of VanBuren et al. (4,5). Only the parameter set (iii) listed in Table 1 obeys the criterion $|E_{lat}| < E_c$, which we found to be crucial for fast disassembly of an energetic driving force. With parameter sets (i), (ii), and (iv) in Table 1, breaking the top ring of lateral bonds (assumed to be the first step of a catastrophe) results in higher energy than the initial state of an intact tube. This is because the gain in curling energy is less than the loss of lateral bond contributions. Then the question naturally arises: what drives fast and continuous disassembly in the absence of permanent external forces? Thermal fluctuations obviously cannot propel depolymerization with a speed 10–20 times greater than MT growth.

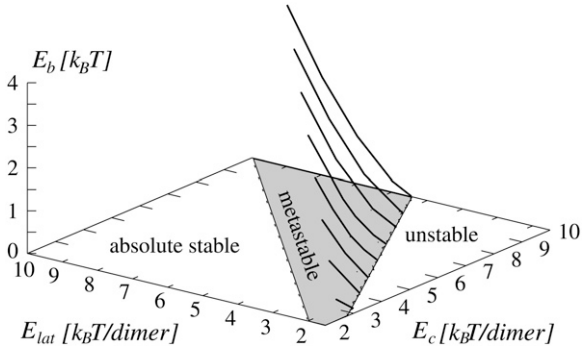

FIGURE 5 Barrier energy E_b (in units of k_BT) as a function of lateral bond energy, E_{lat} (k_BT/dimer) and curling energy, E_c (k_BT/dimer), Lennard-Jones potential, $E_{tot} = -10.5\ k_BT$/dimer. Data are from Table 2. Gray shading indicates the metastable region where the finite energy barrier appears (see Fig. 4).

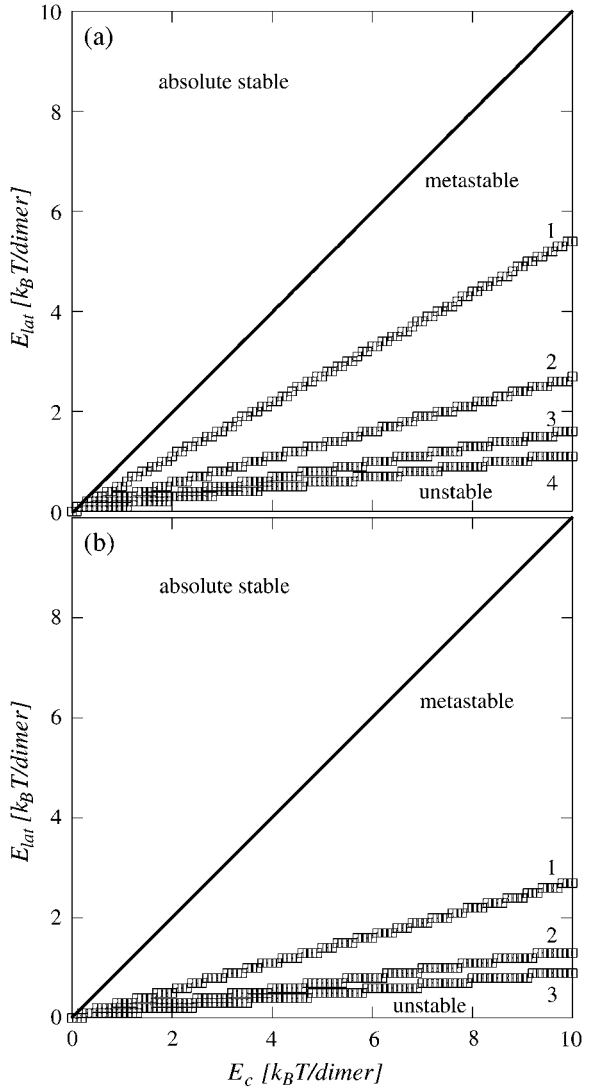

FIGURE 6 Stability diagram for (*a*) Lennard-Jones and (*b*) Morse potential bond representations with different cap lengths (indicated by numbers at the border of metastable regions). $E_{tot} = -10.5\ k_BT$/dimer, and $\delta = 1.12\ nm^{-1}$ for the Morse potential.

Another conclusion was that sheet-like MT tip configurations were much more likely to undergo catastrophes than blunt ends (5), simply because unclosed sheets have many dimers with one-sided lateral bonds. The gain from global structural relaxation (see Jánosi et al. (19), Müller-Reichert et al. (20), and Chrétien et al. (21)) for sheet-like MT tips was not considered in VanBuren et al. (5); however this is important in the energy balance: weaker bond bending frustrations yield to higher energy barriers similarly to the case of

larger GTP caps (see Fig. 4). A quantitative analysis of sheets is not possible in the framework of a single filament approximation, but the results of Molodtsov et al. (6), Jánosi et al. (19), and Chrétien et al. (21) strongly support that structural relaxation increases the stability at the MT terminal.

We thank Collegium Budapest Institute for Advanced Study for access to their computing facilities.

This work was supported by the Hungarian Science Foundation (OTKA) under grant No. TS044839. I.M.J. is grateful for a János Bolyai research scholarship of the Hungarian Academy of Sciences.

REFERENCES

1. Chrétien, D., and S. D. Fuller. 2000. Microtubules switch occasionally into unfavorable configurations during elongation. *J. Mol. Biol.* 298: 663–676.
2. Wang, H.-W., and E. Nogales. 2005. Nucleotide-dependent bending flexibility of tubulin regulates microtubule assembly. *Nature*. 435:911–915.
3. Mitchison, T., and M. Kirschner. 1984. Dynamic instability of microtubule growth. *Nature*. 312:237–242.
4. VanBuren, V., D. J. Odde, and L. Cassimeris. 2002. Estimates of lateral and longitudinal bond energies within the microtubule lattice. *Proc. Natl. Acad. Sci. USA*. 99:6035–6040.
5. VanBuren, V., L. Cassimeris, and D. J. Odde. 2005. Mechanochemical model of microtubule structure and self-assembly kinetics. *Biophys. J.* 89:2911–2926.
6. Molodtsov, M. I., E. A. Ermakova, E. E. Shnol, E. L. Grishchuk, J. R. McIntosh, and F. I. Ataullakhanov. 2005. A molecular-mechanical model of the microtubule. *Biophys. J.* 88:3167–3179.
7. Molodtsov, M. I., E. L. Grishchuk, A. K. Efremov, J. R. McIntosh, and F. I. Ataullakhanov. 2005. Force production by depolymerizing microtubules: a theoretical study. *Proc. Natl. Acad. Sci. USA*. 102:4353–4358.
8. Hunyadi, V., D. Chrétien, and I. M. Jánosi. 2005. Mechanical stress induced mechanism of microtubule catastrophes. *J. Mol. Biol.* 348: 927–938.
9. Erickson, H. P., and E. T. O'Brien. 1992. Microtubule dynamic instability and GTP hydrolysis. *Annu. Rev. Biophys. Biomol. Struct.* 21:145–166.
10. Hyman, A. A., S. Salser, D. N. Drechsel, N. Unwin, and T. J. Mitchison. 1992. Role of GTP hydrolysis in microtubule dynamics: information from a slowly hydrolyzable analogue, GMPCPP. *Mol. Biol. Cell.* 3:1155–1167.
11. Caplow, M., and J. Shanks. 1996. Evidence that a single monolayer tubulin-GTP cap is both necessary and sufficient to stabilize microtubules. *Mol. Biol. Cell.* 7:663–675.
12. Desai, A., and T. J. Mitchison. 1997. Microtubule polymerization dynamics. *Annu. Rev. Cell Dev. Biol.* 13:83–117.
13. Jánosi, I. M., D. Chrétien, and H. Flyvbjerg. 2002. Structural microtubule cap: stability, catastrophe, rescue, and third state. *Biophys. J.* 83:1317–1330.
14. Mitchell, J. B. O., R. A. Laskowski, A. Alex, and J. M. Thornton. 1999. BLEEP—potential of mean force describing protein-ligand interactions: I. Generating potential. *J. Comp. Chem.* 20:1165–1176.
15. Jiang, L., Y. Gao, F. Mao, Z. Liu, and L. Lai. 2002. Potential of mean force for protein-protein interaction studies. *Proteins*. 46:190–196.
16. Sept, D., N. A. Baker, and J. A. McCammon. 2003. The physical basis of microtubule structure and stability. *Protein Sci.* 12:2257–2261.
17. Drabik, P., S. Gusarov, and A. Kovalenko. 2007. Microtubule stability studied by three-dimensional molecular theory of solvation. *Biophys. J.* 92:394–403.
18. Moon, Y. U., R. A. Curtis, C. O. Anderson, H. W. Blanch, and J. M. Prausnitz. 2000. Protein-protein interactions in aqueous ammonium sulfate solutions. Lysozyme and bovine serum albumin (BSA). *J. Solution Chem.* 29:699–718.
19. Jánosi, I. M., D. Chrétien, and H. Flyvbjerg. 1998. Modeling elastic properties of microtubule tips and walls. *Eur. Biophys. J.* 27:501–513.
20. Müller-Reichert, Th., D. Chrétien, F. Severin, and A. A. Hyman. 1998. Structural changes at microtubule ends accompanying GTP hydrolysis: information from a slowly hydrolyzable analogue of GTP, guanylyl (α,β)methylenediphosphonate. *Proc. Natl. Acad. Sci. USA*. 95:3661–3666.
21. Chrétien, D., I. M. Jánosi, J. C. Taveau, and H. Flyvbjerg. 1999. Microtubule's conformational cap. *Cell Struct. Funct.* 24:299–303.